Inorganic Chemistry

Article

pubs.acs.org/IC

Metal–Metal Bonding in Low-Coordinate Dicobalt Complexes Supported by Phosphinoamide Ligands

Ramyaa Mathialagan, Subramaniam Kuppuswamy, Alexandra T. De Denko, Mark W. Bezpalko, Bruce M. Foxman, and Christine M. Thomas*

†Department of Chemistry, Brandeis University, 415 South Street, Waltham, Massachusetts 02451, United States

Supporting Information

ABSTRACT: Homobimetallic dicobalt complexes featuring metal centers in different coordination environments have been synthesized, and their multielectron redox chemistry has been investigated. Treatment of CoX_2 with $MesNKP^iPr_2$ leads to self-assembly of $[(THF)Co(MesNP^iPr_2)_2(\mu\text{-}X)CoX]$ [X = Cl (**1**), I (**2**)], with one Co center bound to two amide donors and the other bound to two phosphine donors. Upon two-electron reduction, a ligand rearrangement occurs to generate the symmetric species $(PMe_3)Co(MesNP^iPr_2)_2Co(PMe_3)$ (**3**), where each Co has an identical mixed P/N donor set. One-electron oxidation of **3** to generate a mixed valence species promotes a ligand rearrangement back to an asymmetric configuration in $[(THF)Co(MesNP^iPr_2)_2Co(PMe_3)][PF_6]$ (**4**). Complexes **1**–**4** have been structurally characterized, and their metal–metal interactions are discussed in the context of computational results.

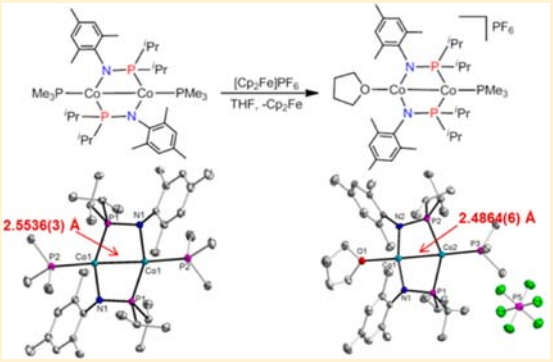

INTRODUCTION

Our group has recently been exploring the metal–metal interactions in heterobimetallic Zr/Co complexes and their effects on redox properties and reactivity.[1] The vastly different electronic natures of the two metals in these systems leads to highly polar metal–metal interactions, shifting the $Co^{I/0}$ and $Co^{0/-I}$ potentials by ca. 1 V with respect to monometallic Co analogues and facilitating reactivity with polar bonds in substrates such as CO_2.[2,3] We were curious to ascertain whether the same enhanced redox properties and reactivity could be imparted by placing the two metals in homobimetallic dicobalt complexes in disparate coordination environments. Similarly, we have recently found that treatment of late metal salts (FeX_2, MnX_2) with phosphinoamide ligands leads to self-assembly of homobimetallic species with each metal center in a different (polyamide vs polyphosphine) coordination environment.[4] Herein, we extend this chemistry to dicobalt systems and uncover some interesting low-coordinate geometries and ligand rearrangements in metal–metal bonded species.

RESULTS AND DISCUSSION

Synthesis and Characterization. The construction of the bimetallic framework was achieved via treatment of cobalt halide salts CoX_2 (X = Cl, I) with an equimolar equivalent of the phosphinoamide potassium salt $MesNKP^iPr_2$. In this manner, the green complexes $[(THF)Co(MesNP^iPr_2)_2(\mu\text{-}X)CoX]$ [X = Cl (**1**), I (**2**)] were obtained in high yield (Scheme 1). Complexes **1** and **2** have similar paramagnetically shifted ^1H NMR spectra with 11 distinct resonances. The apparent inequivalence of many of the phosphinoamide substituents (e.g., four distinct isopropyl-methyl resonances) is indicative of asymmetric complexes (later confirmed by X-ray diffraction). The solution magnetic moments of complexes **1** and **2** were determined using the Evans method [μ_{eff} = 3.0 (**1**) and 3.3 μB (**2**)][5,6] and are lower than would be expected for two high spin Co^{II} centers (spin only value expected for two uncoupled S = 3/2 Co^{II} centers = 6.48 μB), implying some degree of magnetic interaction or bonding between the two Co centers leading to an intermediate spin state.

Scheme 1

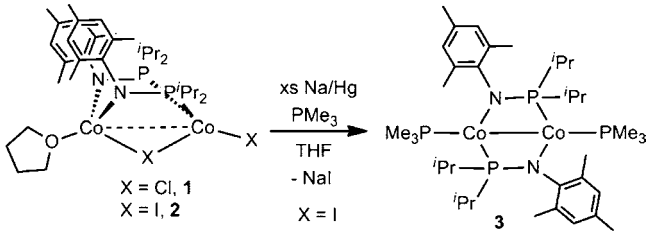

The solid state structures of both **1** and **2** were obtained via X-ray structure analysis of single crystals (Figure 1 and the Supporting Information). Interestingly, the dicobalt complex adopts an asymmetric structure in which one Co^{II} center is coordinated by two amide donors, while the other is bound by two phosphines. This preference was also observed in several other phosphinoamide-linked bimetallic complexes that we

Received: August 22, 2012
Published: January 8, 2013

   dx.doi.org/10.1021/ic3018375 | Inorg. Chem. 2013, 52, 701–706

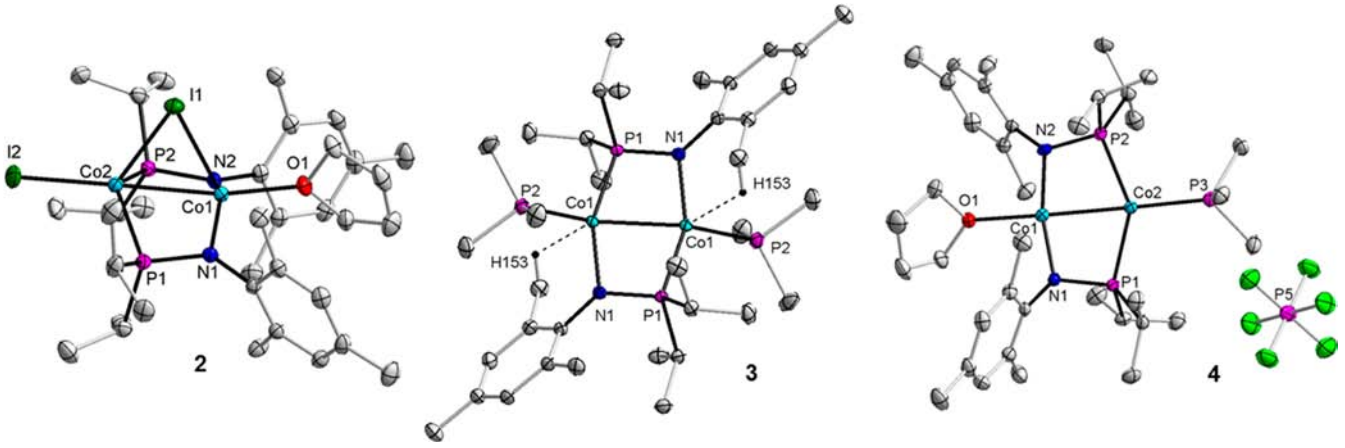

Figure 1. Displacement ellipsoid (50%) representations of **2**, **3**, and **4**. For clarity, only one of two independent molecules in the asymmetric unit of **2** is shown, only one of two disordered PF_6^- positions in **4** is shown, and hydrogen atoms have been omitted. Relevant interatomic distances (Å) and angles (°): **2** (parameters for one of two independent molecules are listed): Co1−Co2, 2.5939(4); Co1−N1, 1.9124(18); Co1−N2, 1.9254(19); Co2−P1, 2.3298(6); Co2−P2, 2.3429(7); Co1−I1, 2.7294(3); Co2−I1, 2.6768(4); Co2−I2, 2.5264(4); Co1−O1, 2.0540(16), Co1−I1−Co2, 57.335(10). **3**: Co1−Co1, 2.5536(3); Co1−P1, 2.1763(3); Co1−P2, 2.2699(3); Co1−N1, 1.9569(8); Co1−Co1−P2, 160.245(11). **4**: Co1−Co2, 2.4864(6); Co1−N1, 1.889(2); Co1−N2, 1.883(2); Co2−P1, 2.2255(9); Co2−P2, 2.2283(9); Co2−P3, 2.2554(9); Co1−O1, 2.063(2).

have recently reported.[4,7] The geometry at each Co center in **2** is distorted pseudotetradrahedral. As a result of the asymmetric coordination environments of the two Co centers, the iodide bridges somewhat asymmetrically, with a slightly longer distance to the amide-bound Co center [2.7294(3) Å vs 2.6768(4) Å]. The short Co−Co distance in **2** is suggestive of a metal−metal bond [2.5939(4) Å and 2.6142(4) Å in two independent molecules in the asymmetric unit of **2**]. Other nonorganometallic $Co^{II}Co^{II}$ complexes with similar metal−metal distances include $Co_2(NR_2)_4$ [R = $SiMe_3$, 2.583(1) Å; R = Ph, 2.566(3) Å],[8,9] while the 3- and 4-fold symmetric amidinato- and triazenato-bridged complexes $Co_2(amidinato)_3^+$ [2.885(1) Å],[10] $Co_2(amidinato)_4$ [2.3735(9) Å],[11] and $Co_2(triazenato)_4$ [2.265(2) Å][12] complexes have much longer and shorter interatomic distances, respectively. Notably, these complexes were also reported to have room temperature magnetic moments indicative of low or intermediate spin states via antiferromagnetic exchange, although no further explanation of the electronic structure was provided.[8−13]

The redox behavior of **2** was investigated using cyclic voltammetry (see Figure 2), revealing multiple reductive events.

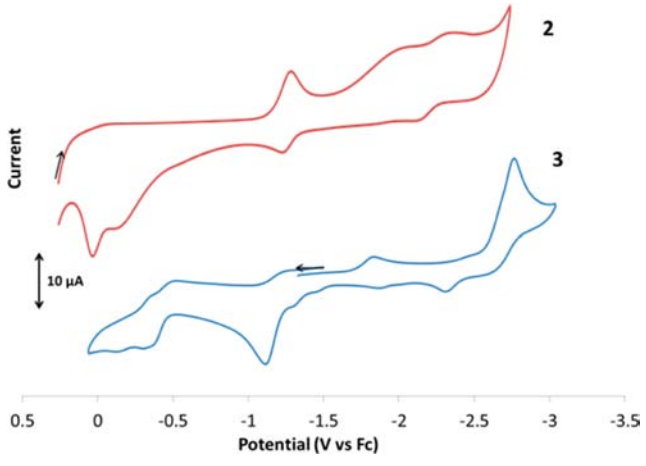

Figure 2. CVs of complexes **2** and **3** (2 mM analyte in 0.4 M [^{n}Bu$_4$N][PF_6] in THF, scan rate = 100 mV/s).

The cyclic voltammogram of complex **2** revealed a well-defined quasi-reversible one-electron reduction at −1.2 V, followed by a series of broad irreversible features at −2.0 and −2.3 V (vs ferrocene). While the reduction at −1.2 V appears fully reversible at scan rates greater than 0.4 V/s, the relative intensity of the return oxidative wave decreases as scan rate is decreased, and at a scan rate of 0.01 V/s, this reduction wave appears entirely irreversible (see the Supporting Information). The quasi-reversible nature of this reductive feature suggests a substantial chemical change in the composition of complex **2** upon reduction.

To investigate these redox processes further, complex **2** was treated with excess Na/Hg amalgam in THF. While this reaction led to an intractable mixture of products, treatment of **2** with Na/Hg in the presence of excess PMe_3 resulted in clean formation of a new red complex, later identified as (PMe_3)-$Co(MesNP^iPr_2)_2Co(PMe_3)$ (**3**), in 63% yield (Scheme 1). The ^{1}H NMR spectrum of **3** remained broad and paramagnetically shifted, but in this case, only six resonances were observed, suggesting a more symmetric structure. X-ray diffraction structure analysis of single crystals of **3** confirmed this observation and revealed that a ligand rearrangement had occurred to generate a complex in which both Co^I centers are in identical coordination environments with one amide and one phosphine donor from the two bridging phosphinoamides (Figure 1). Each Co center is also coordinated by a PMe_3 ligand, and the six-membered $Co_2N_2P_2$ core is rigorously planar. On the basis of the isolated product **3**, ligand rearrangement as well as halide loss may be responsible for the quasi-reversibility of the first reductive feature observed in the CV of **3**. Although it remains unclear how this ligand rearrangement occurs, it seems reasonable that the preferences for a reduced Co^I center for soft phosphine donors might lead to this phenomenon. Indeed, the requirement of excess PMe_3 to promote clean product formation may imply that PMe_3 coordination plays a key role in the ligand rearrangement process.

While the $Co_2N_2P_2$ core of the molecule is planar, the terminal PMe_3 ligands lie 0.93 Å out of this plane. Upon closer inspection, a weak agostic interaction is observed between the

dx.doi.org/10.1021/ic3018375 | Inorg. Chem. 2013, 52, 701−706

Co center and one of the mesityl-methyl hydrogen atoms, and it is likely this interaction that leads to distortion. The hydrogen atom was located in the Fourier difference map and refined, revealing a Co1−H153 distance = 2.327(17) Å and a Co−C−H angle of 120.8°, both indicative of an agostic interaction.[14] Further support for this weak Co−C−H interaction comes from a medium intensity μ(C−H) stretch at 2714 cm^{-1} in the solid state IR spectrum of **3** (see the Supporting Information). Similar weak agostic interactions have been documented in at least one other low-coordinate cobalt complex[15] and are an indicator of the coordinative unsaturation of the two Co centers of **3**.

The metal−metal distance in **3** [2.5536(3) Å] is shorter than that in complexes **1** and **2**, despite the absence of constraints imposed by a monatomic bridging ligand. The Co−Co distance is, however, longer than that observed in the limited number of nonorganometallic $Co^{I}Co^{I}$ complexes in the literature, including $Co_2(PMe_3)_4(\mu\text{-SPh})_2$ [2.3997(5) Å],[16] the amidinate and guanidate dimers $Co_2((ArN)_2CR)_2$ [R = ^{t}Bu, 2.1404(10) Å; R = NCy_2, 2.1345(7) Å],[17] and $(PNP)_2Co_2$ [2.254(1) Å].[18] Much like **1** and **2**, the solution magnetic moment of complex **3** is also significantly lower than would be expected for two high spin Co^{I} centers (μ_{eff} = 2.9 μB vs the expected value of 5.66 μB for two noninteracting Co^{I} centers or 4.90 for a delocalized S = 2 system). This implies that the two Co^{I} centers are either antiferromagnetically coupled or that the electrons on the two metal centers in this highly symmetric complex are delocalized throughout a metal−metal bonded d orbital manifold. The latter explanation is supported by computational results (vide infra).

The cyclic voltammogram of complex **3** (Figure 2) revealed multiple irreversible one-electron redox events, including an oxidation at −1.1 V and a further reduction at −2.7 V (vs Fc/Fc^{+}). On the basis of the mild oxidation potential of **3**, attempts were made to carefully oxidize this complex to obtain a mixed valence complex. Treatment of **3** with 1 equiv of $[Cp_2Fe][PF_6]$ resulted in a mixed valence complex $[(THF)Co(MesNP^iPr_2)_2\text{-}Co(PMe_3)][PF_6]$ (**4**) in which the phosphinoamide had again unexpectedly rearranged to adopt a structure in which one Co center was bound to two phosphines and the other was ligated by two amides (Scheme 2). Notably, treatment of **3** with 2

Scheme 2

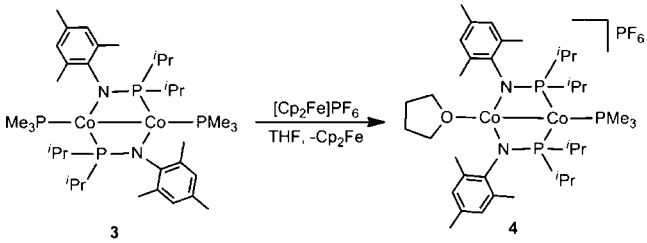

equiv of $[Cp_2Fe][PF_6]$ in attempts to generate a halide-free dicobalt(II) complex led to isolation of the monometallic Co^{II} complex $[Co(MesNP^iPr_2)(PMe_3)_3]PF_6$ (**5**, see the Supporting Information).

The paramagnetically shifted ^{1}H NMR of **4** revealed nine distinct resonances, suggesting a relatively symmetric structure. The solid state structure of **4** (Figure 1) reveals that PMe_3 remains coordinated to the phosphine-bound Co center, while THF coordinates to the amide-ligated Co ion. In this mixed valence complex, the Co−Co separation is contracted even further to 2.4864(6) Å, in line with other nonorganometallic $Co^{II}Co^{I}$ complexes in the literature: $Co_2(amidinato)_3$ [2.385(1) Å, 2.3201(9) Å],[10] $[Co_2(SAr)_5]^-$ [2.511(4) Å],[19] and $Co_2(\mu\text{-}^tBu_2P)_2Cl(PMe_3)_2$ [2.508(2) Å].[20] As might be expected based on the magnetic moment of precursor complex **3**, the solution magnetic moment of complex **4** is sufficiently low to indicate distribution of the metal d electrons throughout a metal−metal bonding manifold (μ_{eff} = 1.4 μ_B). Furthermore, the solution EPR spectrum of **4** (77 K, X-band) is indicative of an S = 1/2 system (see the Supporting Information). Again, it is difficult to speculate on how the ligand rearrangement occurs upon oxidation from **3** to **4**, but the driving force may be that the oxidized Co^{II} center would be more likely to prefer π-donating amide donors than a Co^{I} center. This implies an assignment of the amide-ligated Co center as Co^{II} in this mixed valence $Co^{II}Co^{I}$ complex, and such an assignment is consistent with computational predictions (vide infra).

To further address the metal−metal interactions in complex **4**, UV−vis-NIR data were collected. As shown in Figure 3, the

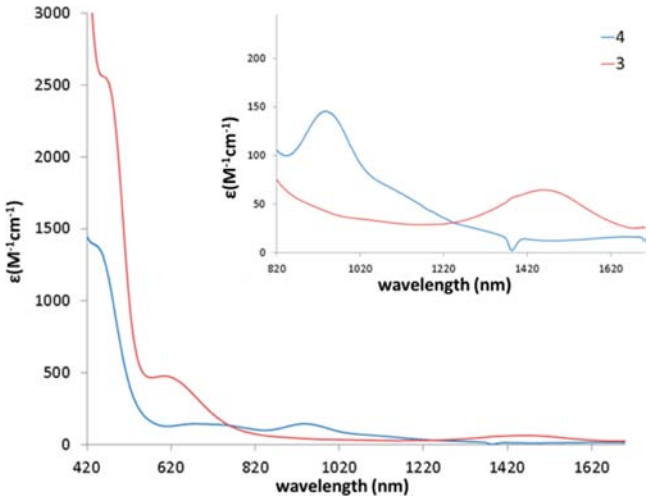

Figure 3. UV−vis-NIR spectra of **3** and **4** (in THF solution). The inset shows an expanded view of the near-infrared region of the spectrum.

UV−vis-NIR spectrum of **4** has a number of low intensity transitions in the 650−950 nm range, including a somewhat broad low intensity band at 949 nm (ε = 140 M^{-1} cm^{-1}). Because complex **4** is formally a mixed valence $Co^{II}Co^{I}$ system, this band could reasonably be assigned as an intervalence charge transfer (IVCT) band, and the asymmetric coordination environments of the two cobalt centers might be expected to increase the energy of this transition into the visible range. Given the metal−metal bonding and the degree of orbital mixing in complex **4**, however (vide infra), such an interpretation may be oversimplified in this case. For comparison, the UV−vis-NIR spectrum of the symmetric $Co^{I}Co^{I}$ complex **3** is also shown in Figure 3. This spectrum is less complex than that of **4**, with a very broad low intensity feature centered at 1476 nm (ε = 64 M^{-1} cm^{-1}), which can likely be attributed to a d−d transition within the metal−metal bonding orbital manifold.

Computational Investigation. To further investigate the electronic structure and metal−metal bonding in the planar dicobalt complexes **3** and **4**, a computational investigation was conducted using density functional theory (DFT) methods

dx.doi.org/10.1021/ic3018375 | Inorg. Chem. 2013, 52, 701−706

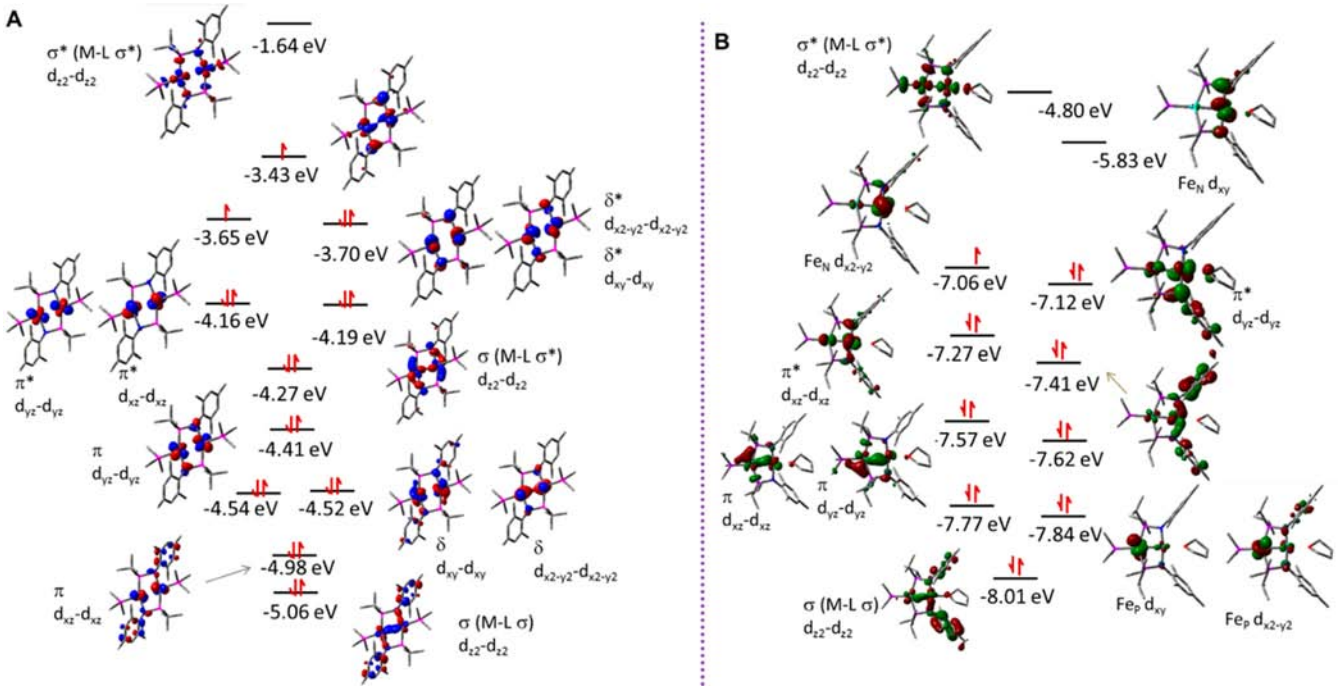

Figure 4. Frontier molecular orbital diagram of (A) **3** and (B) **4** [BP86/LANL2TZ(f)/6-311+G(d)/D95V].

[BP86/LANL2TZ(f)/6-311+G(d)/D95 V]. Solution magnetic moment data for complexes **3** and **4** indicate triplet and doublet configurations, respectively. Nonetheless, geometry optimizations were performed on both molecules in all possible spin states (triplet and quintet for **3**; doublet, quartet, and sextet for **4**). Comparison of the optimized geometries computed for these various spin states with the solid state optimized geometries obtained for these two complexes using X-ray crystallography reveals that the best prediction is obtained with the $S = 1$ (**3**) and $S = 1/2$ (**4**) configurations (see the Supporting Information).

The frontier molecular orbital diagram of **3** reveals both metal−metal σ and π interactions, as shown in Figure 4A. As a result of substantial phosphinoamide ligand contributions, 12 MOs with metal orbital contributions are shown in the figure. There are three orbitals comprised of metal−metal σ interactions, including a low-lying metal−metal σ bonding orbital (−5.06 eV) that is also σ bonding with respect to the metal−amide bonds, a metal−metal σ bond that is σ^* with respect to the metal−amide bonds (−4.27 eV), and the LUMO (−1.64 eV), which is σ^* with respect to the metal−metal interaction as well as the metal−ligand interactions. Additional δ and π interactions between the two Co centers are also present, with the symmetry partially disrupted by the two different ligand donors on each Co ion. The LUMO is sufficiently higher in energy than the remaining occupied orbitals in the metal−metal bonding manifold, resulting in an intermediate spin ($S = 1$) ground state. On the basis of the MO diagram shown in Figure 4, the Co−Co bond order is estimated to be ca. 1.

More information about the bonding between the cobalt centers was obtained via natural bond orbital (NBO)[21] analysis and Mayer population analysis.[22] The Co−Co Wiberg bond indices calculated for **3** and **4** (0.54 and 0.51, respectively) are nearly identical (Table 1), while calculations suggest that the Mayer bond order for **3** is slightly higher than that of **4**. While the absolute values of these computed bond orders are difficult to interpret, comparison of the Co−Co bond orders calculated for these two molecules is a useful exercise and indicates that the metal−metal bond in **3** is stronger than that in **4**.

Table 1. Natural Charges and Wiberg Bond Indices (WBIs) Calculated for 3 and 4 Using NBO Calculations and Calculated Mayer Bond Orders (MBOs)

	Nat charge			
	Co1	Co2	Co−Co WBI	Co−Co (MBO)
3	−0.16	−0.16	0.54	0.98
4	0.62 (CoN)	−0.23 (CoP)	0.51	0.80

NBO analysis reveals that the Co−Co σ bond in **3** is covalent in nature, with 50% orbital contributions from each Co center (for both α and β NBOs, see the Supporting Information). This is consistent with the identical coordination environments and equivalent natural charges of the two metal centers (Table 1). In contrast, the Co centers in the asymmetric mixed valence molecule **4** have vastly different natural charges, with the amide-bound Co center significantly more positively charged than either the phosphine bound Co atom or the two Co centers in starting material **3**. In this case, there is poorer orbital overlap between the two different Co centers because of mismatched orbital energies, as illustrated in the calculated frontier MO diagram shown in Figure 4B. There are no apparent δ interactions, and the π interactions are weaker and more polarized. Nonetheless, the Co−Co σ bond remains relatively covalent (α NBO: 29% Co_N, 71% Co_P; β NBO: 75% Co_N, 28% Co_P). As a result, the overall Co−Co bond order in **4** remains ∼1, although the bond may be slightly weaker than that in **3** as a result of mismatched orbital energies.

■ CONCLUSION

In summary, the $[MesNP^iPr_2]^-$ ligand supports low-coordinate dicobalt dimers with significant metal−metal bonding. The orientation of the ligands in these complexes is highly dependent on the overall redox state of the dicobalt unit.

dx.doi.org/10.1021/ic3018375 | *Inorg. Chem.* 2013, 52, 701−706

Future studies will focus on the reactivity of the reduced complex **3** toward small molecule activation.

EXPERIMENTAL SECTION

General Considerations. Unless specified otherwise, all manipulations were performed under an inert atmosphere using standard Schlenk or glovebox techniques. Glassware was oven-dried before use. Benzene, pentane, diethyl ether, tetrahydrofuran, and toluene were dried using a Glass Contours solvent purification system. All solvents were stored over 3 Å molecular sieves prior to use. Benzene-d_6 (Cambridge Isotopes) was degassed via repeated freeze−pump−thaw cycles and dried over 3 Å molecular sieves. THF-d_8 was dried over CaH_2, vacuum-transferred, and degassed via repeated freeze−pump−thaw cycles. MesNKP^{i}Pr$_2$ was synthesized using literature procedures.[2,4] Anhydrous $CoCl_2$ and CoI_2 were purchased from Strem Chemicals and used after 12 h of drying at 100 °C under vacuum. NMR spectra were recorded at ambient temperature on a Varian Inova 400 MHz instrument. Chemical shifts are reported in δ (ppm). For ^{1}H and ^{13}C{^{1}H} NMR spectra, the solvent resonance was used as an internal reference, and for ^{31}P{^{1}H} NMR spectra, 85% H_3PO_4 was referenced as an external standard (0 ppm). IR spectra were recorded on a Varian 640-IR spectrometer controlled by Resolutions Pro software. UV−vis spectra were recorded on either a Cary 50 UV−vis or Cary 5000 UV−vis-NIR spectrophotometer using Cary WinUV software. Elemental analyses were performed at Complete Analysis Laboratory Inc. (Parsippany, NJ). Solution magnetic moments were measured using Evans' method.[5,6]

X-ray Crystallography. All operations were performed on a Bruker-Nonius Kappa Apex2 diffractometer, using graphite monochromated Mo Kα radiation. All diffractometer manipulations, including data collection, integration, scaling, and absorption corrections, were carried out using the Bruker Apex2 software.[23] Preliminary cell constants were obtained from three sets of 12 frames. Fully labeled diagrams and data collection and refinement details are included in Table S1 and on pages S18−S31 in the Supporting Information.

Computational Details. All calculations were performed using Gaussian09, Revision A.02, for the Linux operating system.[24] Density functional theory calculations were carried out using a combination of Becke's 1988 gradient-corrected exchange functional[25] and Perdew's 1986 electron correlation functional[26] (BP86). A mixed basis set was employed, using the LANL2TZ(f) triple-ζ basis set with effective core potentials for cobalt,[27,28] Gaussian09's internal 6-311+G(d) for heteroatoms (nitrogen, oxygen, phosphorus), and Gaussian09's internal LANL2DZ basis set (equivalent to D95 V[29]) for carbon and hydrogen. Using crystallographically determined geometries as a starting point, the geometries were optimized to a minimum, followed by analytical frequency calculations to confirm that no imaginary frequencies were present. Mayer bond analysis was performed with the routines included in the Gaussian09 software package,[22] and Wiberg bond indices and NBO calculations were carried out using Gaussian NBO Version 3.1.[21]

Electrochemistry. CV measurements were carried out in a glovebox under a dinitrogen atmosphere in a one-compartment cell using a CH Instruments electrochemical analyzer. A glassy carbon electrode and platinum wire were used as the working and auxiliary electrodes, respectively. The reference electrode was Ag/$AgNO_3$ in THF. Solutions of electrolyte (0.40 M [^{n}Bu$_4$N][PF_6] in THF) and analyte (2 mM) were also prepared in the glovebox. All potentials are reported versus an internal ferrocene/ferrocenium reference.

Synthesis of [(THF)Co(MesNP^{i}Pr$_2$)$_2$(μ-Cl)CoCl] (1). A solution of MesNKP^{i}Pr$_2$ (0.28 g, 1.0 mmol) in THF (3 mL) was cooled to −32 °C and this was added to $CoCl_2$ (0.130 g, 1.00 mmol) in THF (2 mL) dropwise over 5 min. The resulting mixture was gradually allowed to warm to room temperature and continuously stirred for 12 h. The insoluble materials were removed by filtration through Celite, and all volatiles were subsequently removed from the filtrate in vacuo. The resulting green material was extracted with diethyl ether (4 × 2 mL) and filtered to remove the byproduct, KCl, and other insoluble impurities. Upon standing at room temperature, the concentrated ether solution of **1** yielded analytically pure **1** as green blocks (0.36 g, 95%). ^{1}H NMR (400 MHz, C_6D_6): δ 26.3 (6H, iPr-Me), 17.0 (2H, Mes), 12.3 (2H, Mes), 9.3 (6H, Mes-Me), 6.7 (6H, Mes-Me), 4.3 (6H, iPr-Me), 2.9 (6H, Mes-Me), −4.2 (6H, iPr-Me), −4.9 (4H, THF), −8.0 (6H, iPr-Me), −11.4 (4H, THF) (isopropyl-methine proton is not observed because of its close proximity to the paramagnetic Co center, tentative assignments based on relative integration). UV−vis (C_6H_6) λ_{max}, nm (ε, L mol^{-1} cm^{-1}): 450 (390), 506 (230), 365 (910), 670 (730). Evans' method (C_6D_6): 2.98 μ_B. Anal. calcd for $C_{34}H_{58}Co_2N_2P_2OCl_2$: C, 53.62; H, 7.68; N, 3.69. Found: C, 53.53; H, 7.79; N, 3.75.

Synthesis of (THF)Co(MesNP^{i}Pr$_2$)$_2$(μ-I)CoI (2). A solution of MesNKP^{i}Pr$_2$ (0.85 g, 3.0 mmol) was cooled to −32 °C in THF (15 mL) and this was added to CoI_2 (0.94 g, 3.0 mmol) in THF (10 mL) dropwise over 5 min. The resulting mixture was gradually allowed to warm to room temperature and continuously stirred for 12 h. The insoluble materials were removed by filtration through Celite, and all volatiles were subsequently removed from the filtrate in vacuo. The resulting green material was extracted with diethyl ether (4 × 5 mL) and filtered to remove the byproduct, KI, and other insoluble impurities. Concentration of this diethyl ether solution and storage at −32 °C afforded analytically pure **2** as green blocks (0.92 g, 66%). ^{1}H NMR (400 MHz, C_6D_6): δ 24.5 (6H, iPr-Me), 15.8 (2H, Mes), 11.7 (2H, Mes), 10.0 (6H, Mes-Me), 7.9 (6H, Mes-Me), 5.3 (6H, iPr-Me), 1.9 (6H, Mes-Me), −2.9 (6H, iPr-Me), −5.7 (4H, THF), −10.6 (6H, iPr-Me), −11.7 (4H, THF) (isopropyl-methine proton is not observed because of its close proximity to the paramagnetic Co center, tentative assignments based on relative integration). UV−vis (C_6H_6) λ_{max}, nm (ε, L mol^{-1} cm^{-1}): 364 (440), 608 (640), 688 (860), 746 (610). Evans' method (C_6D_6): 3.29 μ_B. Anal. calcd for $C_{34}H_{58}Co_2N_2P_2I_2$: C, 43.24; H, 6.19; N, 2.97. Found: C, 43.30; H, 6.29; N, 3.04.

Synthesis of (PMe$_3$)Co(MesNP^{i}Pr$_2$)$_2$Co(PMe$_3$) (3). A 0.5% Na/Hg amalgam was prepared from 0.003 g of Na (0.1 mmol) and 0.6 g of Hg. To this vigorously stirred amalgam in 10 mL of THF was added a cold (−32 °C) solution of **2** (0.047 g, 0.050 mmol) in THF (5 mL). Neat PMe_3 (26 μL, 0.20 mmol) was added to the reaction mixture immediately, and the solution rapidly changed from green to brick red in color. After it was stirred for 2.5 h, the resulting red solution was decanted from the amalgam and filtered through Celite. Volatiles were removed from the filtrate in vacuo. The resulting red material was extracted with diethyl ether (4 × 2 mL) to remove NaI and other insoluble impurities. Upon concentration of this diethyl ether solution of **3** followed by storage at room temperature for 12 h, dark reddish brown single crystals of **3** were obtained (0.024 g, 63%). ^{1}H NMR (400 MHz, C_6D_6): δ 10.6 (6H, Mes-Me), 7.9 (18H, PMe_3), 4.2 (12H, Mes-Me), 0.3 (4H, Mes), −6.2 (12H, iPr-Me), −9.0 (12H, iPr-Me) (isopropyl-methine proton is not observed because of its close proximity to the paramagnetic Co center, tentative assignments based on relative integration). UV−vis (C_6H_6) λ_{max}, nm (ε, L mol^{-1} cm^{-1}): 471 (2500), 623 (470), 1476 (64). Evans' method (C_6D_6): 2.86 μ_B. Anal. calcd for $C_{36}H_{68}Co_2N_2P_4$: C, 56.10; H, 8.89; N, 3.63. Found: C, 56.11; H, 8.94; N, 3.73.

Synthesis of [(THF)Co(MesNP^{i}Pr$_2$)$_2$Co(PMe$_3$)]PF$_6$ (4). A solution of **3** (0.039 g, 0.050 mmol) in THF (3 mL) was cooled to −32 °C for 30 min, and this solution was added to a THF (2 mL) solution of $FcPF_6$ (0.017 g, 0.050 mmol). The reaction progress was monitored by ^{1}H NMR spectroscopy, and after 2 h of stirring the mixture at rt, the starting material had cleanly converted to a new compound. At this point, the solution was filtered through Celite to remove insoluble materials. The volatiles were removed from the filtrate in vacuo, and this material was washed with pentane to remove ferrocene and other byproducts. The remaining orange material was redissolved in THF (2 mL), layered with pentane (3 mL), and stored at room temperature, resulting in orange blocks of **4** along with a small amount of [Co(PMe_3)$_4$]PF_6 as a minor byproduct. Complex **4** was isolated by manual separation from the mixture (0.039 g, 29%). ^{1}H NMR (400 MHz, C_6D_6): δ 80.5 (4H, THF), 32.3 (Mes-Me), 20.3 (4H, THF), 17.0 (9H, PMe_3), 1.2 (12H, Mes-Me), −7.6 (12H, iPr-Me), −10.0 (12H, very broad, Mes), −17.4 (iPr-Me) (isopropyl-

dx.doi.org/10.1021/ic3018375 | Inorg. Chem. 2013, 52, 701−706

methine proton is not observed because of its close proximity to the paramagnetic Co center, tentative assignments based on relative integration). UV−vis (C_6H_6) λ_{max}, nm (ε, L mol^{-1} cm^{-1}): 454 (1300), 682 (150), 728 (140), 949 (140). Evans' method (C_6D_6): 1.45 μ_B. Complex **4** is thermally unstable in both solution and the solid state—it is likely for this reason that the solution magnetic data are artificially low and satisfactory combustion analysis data could not be obtained.

Synthesis of [Co(MesNP^{i}Pr$_2$)(PMe$_3$)$_3$]PF$_6$ (5). A solution of **3** (0.039 g, 0.050 mmol) in THF (3 mL) was cooled to −32 °C for 30 min, and this was added to a THF (2 mL) solution of $FcPF_6$ (0.033 g, 0.10 mmol). The reaction progress was monitored by ^{1}H NMR spectroscopy; the starting materials were completely converted to a new compound after 2 h of stirring the reaction mixture at rt. The solution was filtered through Celite to remove insoluble materials. Volatiles were removed from the filtrate, and the orange material was subsequently washed with pentane to remove ferrocene and other byproducts. The remaining orange material was redissolved in THF (2 mL), layered with pentane (3 mL), and stored at room temperature, resulting in orange blocks of **5** (0.038 g, 40%). ^{1}H NMR (400 MHz, C_6D_6): δ 18.9 (2H, Mes), 1.8 (27H, PMe_3), 1.3 (3H, Mes-Me), −1.7 (6H, iPr-Me), −2.4 (6H, Mes-Me), −8.0 (6H, iPr-Me) (isopropyl-methine proton is not observed because of its close proximity to the paramagnetic Co center, tentative assignments based on relative integration). UV−vis (C_6H_6) λ_{max}, nm (ε, L mol^{-1} cm^{-1}): 450 (1400), 671 (380). Evans' method (C_6D_6): 3.53 μ_B. Anal. calcd for $C_{37}H_{67}Co_2N_2P_5F_{12}$: C, 42.70; H, 6.49; N, 2.69. Found: C, 43.23; H, 7.96; N, 1.85.

■ ASSOCIATED CONTENT

Ⓢ Supporting Information

Spectroscopic and cyclic voltammetry data, crystallographic and computational details, and crystallographic data in CIF format. This material is available free of charge via the Internet at http://pubs.acs.org.

■ AUTHOR INFORMATION

Corresponding Author

*E-mail: thomasc@brandeis.edu.

Notes

The authors declare no competing financial interest.

■ ACKNOWLEDGMENTS

This manuscript is based on work supported by the U.S. Department of Energy (DE-SC0004019). C.M.T. is grateful for a 2011 Alfred P. Sloan Fellowship. We thank Jeremy P. Krogman for assistance with X-ray structure determination and Dr. Casey R. Wade for assistance with UV−vis-NIR measurements.

■ REFERENCES

(1) Thomas, C. M. *Comments Inorg. Chem.* **2011**, *32*, 14−38.
(2) Greenwood, B. P.; Forman, S. I.; Rowe, G. T.; Chen, C.-H.; Foxman, B. M.; Thomas, C. M. *Inorg. Chem.* **2009**, *48*, 6251−6260.
(3) Krogman, J. P.; Foxman, B. M.; Thomas, C. M. *J. Am. Chem. Soc.* **2011**, *133*, 14582−14585.
(4) Kuppuswamy, S.; Bezpalko, M. W.; Powers, T. M.; Turnbull, M. M.; Foxman, B. M.; Thomas, C. M. *Inorg. Chem.* **2012**, *51*, 8225−8240.
(5) Sur, S. K. *J. Magn. Reson.* **1989**, *82*, 169−173.
(6) Evans, D. F. *J. Chem. Soc.* **1959**, 2003−2005.
(7) Kuppuswamy, S.; Cooper, B. G.; Bezpalko, M. W.; Foxman, B. M.; Powers, T. M.; Thomas, C. M. *Inorg. Chem.* **2012**, *51*, 1866−1873.
(8) Murray, B. D.; Power, P. P. *Inorg. Chem.* **1984**, *23*, 4584−4588.
(9) Hope, H.; Olmstead, M. M.; Murray, B. D.; Power, P. P. *J. Am. Chem. Soc.* **1985**, *107*, 712−713.
(10) Cotton, F. A.; Daniels, L. M.; Maloney, D. J.; Matonic, J. H.; Murillo, C. A. *Inorg. Chim. Acta* **1997**, *256*, 283−289.
(11) Cotton, F. A.; Daniels, L. M.; Feng, X.; Maloney, D. J.; Matonic, J. H.; Murilio, C. A. *Inorg. Chim. Acta* **1997**, *256*, 291−301.
(12) Cotton, F. A.; Poli, R. *Inorg. Chem.* **1987**, *26*, 3652−3653.
(13) Theopold, K. H.; Silvestre, J.; Byrne, E. K.; Richeson, D. S. *Organometallics* **1989**, *8*, 2001−2009.
(14) Brookhart, M.; Green, M. L. H.; Parkin, G. *Proc. Natl. Acad. Sci. U.S.A.* **2007**, *104*, 6908−6914.
(15) Olmstead, M. M.; Power, P. P.; Sigel, G. *Inorg. Chem.* **1986**, *25*, 1027−1033.
(16) Jiao, G.; Li, X.; Sun, H.; Xu, X. *J. Organomet. Chem.* **2007**, *692*, 4251−4258.
(17) Jones, C.; Schulten, C.; Rose, R. P.; Stasch, A.; Aldridge, S.; Woodul, W. D.; Murray, K. S.; Moubaraki, B.; Brynda, M.; La; Macchia, G.; Gagliardi, L. *Angew. Chem., Int. Ed.* **2009**, *48*, 7406−7410.
(18) Fout, A. R.; Basuli, F.; Fan, H.; Tomaszewski, J.; Huffman, J. C.; Baik, M.-H.; Mindiola, D. J. *Angew. Chem., Int. Ed.* **2006**, *45*, 3291−3295.
(19) Ruhlandt-Senge, K.; Power, P. P. *J. Chem. Soc., Dalton Trans.* **1993**, 649−650.
(20) Jones, R. A.; Stuart, A. L.; Atwood, J. L.; Hunter, W. E.; Rogers, R. D. *Organometallics* **1982**, *1*, 1721−1723.
(21) Glendening, E. D.; Reed, A. E.; Carpenter, J. E. *NBO Version 3.1*.
(22) Mayer, I. *Int. J. Quantum Chem.* **1986**, *29*, 477−483.
(23) *Apex 2: Version 2 User Manual, M86-E01078*; Bruker Analytical X-ray Systems: Madison, WI, 2006.
(24) Frisch, M. J.; Trucks, G. W.; Schlegel, H. B.; Scuseria, G. E.; Robb, M. A.; Cheeseman, J. R.; Scalmani, G.; Barone, V.; Mennucci, B.; Petersson, G. A.; Nakatsuji, H.; Caricato, M.; Li, X.; Hratchian, H. P.; Izmaylov, A. F.; Bloino, J.; Zheng, G.; Sonnenberg, J. L.; Hada, M.; Ehara, M.; Toyota, K.; Fukuda, R.; Hasegawa, J.; Ishida, M.; Nakajima, T.; Honda, Y.; Kitao, O.; Nakai, H.; Vreven, T.; Montgomery, J. A., Jr.; Peralta, J. E.; Ogliaro, F.; Bearpark, M.; Heyd, J. J.; Brothers, E.; Kudin, K. N.; Staroverov, V. N.; Kobayashi, R.; Normand, J.; Raghavachari, K.; Rendell, A.; Burant, J. C.; Iyengar, S. S.; Tomasi, J.; Cossi, M.; Rega, N.; Millam, J. M.; Klene, M.; Knox, J. E.; Cross, J. B.; Bakken, V.; Adamo, C.; Jaramillo, J.; Gomperts, R.; Stratmann, R. E.; Yazyev, O.; Austin, A. J.; Cammi, R.; Pomelli, C.; Ochterski, J. W.; Martin, R. L.; Morokuma, K.; Zakrzewski, V. G.; Voth, G. A.; Salvador, P.; Dannenberg, J. J.; Dapprich, S.; Daniels, A. D.; Farkas, O.; Foresman, J. B.; Ortiz, J. V.; Cioslowski, J.; Fox, D. J. *Gaussian 09*, revision A.2; Gaussian, Inc.: Wallingford, CT, 2009.
(25) Becke, A. D. *Phys. Rev. A* **1988**, *38*, 3098−3100.
(26) Perdew, J. P. *Phys. Rev. B* **1986**, *33*, 8822−8824.
(27) Hay, P. J.; Wadt, W. R. *J. Chem. Phys.* **1985**, *82*, 299−310.
(28) Hay, P. J.; Wadt, W. R. *J. Chem. Phys.* **1985**, *82*, 270−283.
(29) Dunning, T. H.; Hay, P. J. In *Modern Theoretical Chemistry*; Schaefer, H. F., Ed.; Plenum: New York, 1976; Vol. 3, pp 1−28.